International Journal of Nanomedicine

Dovepress
open access to scientific and medical research

Open Access Full Text Article

ORIGINAL RESEARCH

# Dual UV irradiation-based metal oxide nanoparticles for enhanced antimicrobial activity in *Escherichia coli* and M13 bacteriophage



This article was published in the following Dove Press journal:
International Journal of Nanomedicine
1 November 2017
Number of times this article has been viewed

Su-Eon Jin[1]
Woochul Hwang[2]
Hyo Jung Lee[3]
Hyo-Eon Jin[3]

[1]Research Institute for Medical Sciences, College of Medicine, Inha University, Incheon, [2]ECOSET Co., Ltd., Ansan, [3]College of Pharmacy, Ajou University, Suwon, Korea

**Abstract:** Metal oxide (MO) nanoparticles have been studied as nano-antibiotics due to their antimicrobial activities even in antibiotic-resistant microorganisms. We hypothesized that a hybrid system of dual UV irradiation and MO nanoparticles would have enhanced antimicrobial activities compared with UV or MO nanoparticles alone. In this study, nanoparticles of ZnO, $ZnTiO_3$, MgO, and CuO were selected as model nanoparticles. A dual UV collimated beam device of UV-A and UV-C was developed depending upon the lamp divided by coating. Physicochemical properties of MO nanoparticles were determined using powder X-ray diffractometry (PXRD), Brunauer-Emmett-Teller analysis, and field emission-scanning electron microscopy with energy-dispersive X-ray spectroscopy. Atomic force microscopy with an electrostatic force microscopy mode was used to confirm the surface topology and electrostatic characteristics after dual UV irradiation. For antimicrobial activity test, MO nanoparticles under dual UV irradiation were applied to *Escherichia coli* and M13 bacteriophage (phage). The UV-A and UV-C showed differential intensities in the coated and uncoated areas (UV-A, coated = uncoated; UV-C, coated << uncoated). MO nanoparticles showed sharp peaks in PXRD patterns, matched to pure materials. Their primary particle sizes were less than 100 nm with irregular shapes, which had an 8.6~25.6 $m^2/g$ of specific surface area with mesopores of 22~262 nm. The electrostatic properties of MO nanoparticles were modulated after UV irradiation. ZnO, MgO, and CuO nanoparticles, except $ZnTiO_3$ nanoparticles, showed antibacterial effects on *E. coli*. Antimicrobial effects on *E. coli* and phages were also enhanced after cyclic exposure of dual UV and MO nanoparticle treatment using the uncoated area, except ZnO nanoparticles. Our results demonstrate that dual UV-MO nanoparticle hybrid system has a potential for disinfection. We anticipate that it can be developed as a next-generation disinfection system in pharmaceutical industries and water purification systems.

**Keywords:** dual UV, metal oxide nanoparticles, antimicrobial activity, *E. coli*, M13 bacteriophage

## Introduction

Metal oxide (MO) nanoparticles have antimicrobial activities, which are so called "nano-antibiotics", and are used in various research fields including environmental, pharmaceutical, and biomedical applications.[1–3] Compared with conventional antibiotic drugs or disinfection agents, MO nanoparticles show enhanced disinfection potentials, even in antibiotic-resistant microorganisms.[1,2] Under UV irradiation, they also target microorganisms and enhance the antimicrobial activities as disinfection agents in a purification system.[4,5] Thus, the combination of UV and MO nanoparticles can be applied for a future disinfection system.[6,7]

Correspondence: Su-Eon Jin
Research Institute for Medical Sciences, College of Medicine, Inha University, 100 Inha-ro, Nam-gu, Incheon, 22332, Korea
Email jins@inha.ac.kr

Hyo-Eon Jin
College of Pharmacy, Ajou University, 206 Worldcup-ro, Yeongtong-gu, Suwon, 16499, Korea
Email hjin@ajou.ac.kr

submit your manuscript | www.dovepress.com
Dovepress
http://dx.doi.org/10.2147/IJN.S144236

In dual UV-MO nanoparticle hybrid system, MO nanoparticles are highlighted by their surface characteristics, physicochemical properties,[8] and photocatalytic activity.[9–11] Adsorption function of MO nanoparticles to microorganisms can induce the disruption of bio-membranes and massive leakage of cell contents, due to their surface characteristics and physicochemical properties.[12] MO nanoparticles also have disinfection potential under UV irradiation, as well as in dark conditions.[13–15] They generate reactive oxygen species (ROS) as photocatalysts over wavelength ranges of band gap energies, and induce ROS-mediated toxicity and decomposition in microorganisms after UV treatment.[11,14–17]

UV irradiation has been studied as an alternative disinfection technique in purification systems, as well as clinics.[17–19] In the UV spectra, UV-C (100~280 nm) is generally used for disinfection, which is lethal in bacteria and inactivates viruses due to its damage to genetic materials by absorption at 250~270 nm as a peak germicidal wavelength.[18] UV-A (315~400 nm) also induces ROS production and leads to oxidative cell damage,[19] which is applied as an insecticide at longer exposure. UV-A affects the survival rate in immature stages of worms.[17] Thus, dual UV irradiation of UV-A and UV-C can be a wide spectrum disinfection agent in a hybrid system with MO nanoparticles.

In this study, we report on a dual UV-MO nanoparticle hybrid system combining UV-A and UV-C to enhance antimicrobial activities (Figure 1). MO nanoparticles of ZnO, $ZnTiO_3$, MgO, and CuO were selected. Physicochemical properties of MO nanoparticles were determined and antimicrobial activities of the hybrids were confirmed in *Escherichia coli* and M13 bacteriophages (phage). First, crystallinity, and pore size of MO nanoparticles were confirmed using powder X-ray diffractometry (PXRD), and Brunauer-Emmett-Teller (BET) analysis. Morphology and elemental compositions were investigated using field emission-scanning electron microscopy (FE-SEM) with energy-dispersive X-ray spectroscopy (EDS). Surface characteristics and electrostatic properties of MO nanoparticles were monitored using atomic force microscopy (AFM), and electrostatic force microscopy (EFM). For dual-UV irradiation, a collimated beam device (CBD) was used with a dual UV lamp divided into coated and uncoated areas, respectively. UV spectra were monitored using a spectrometer.

# Experimental

## Chemical reagents

MO nanoparticles of ZnO, $ZnTiO_3$, MgO, and CuO were purchased from Sigma-Aldrich Co. (St Louis, MO, USA). Isopropyl alcohol and absolute ethanol (99.9%) were obtained from Sigma-Aldrich Co. Luria-Bertani (LB) medium and agar were obtained from BD Biosciences (San Jose, CA, USA). All chemicals were of reagent grade without further purification. Deionized water was obtained using a Milli-Q water purification system (EMD Millipore, Billerica, MA, USA).

## Dual UV in CBD

CBD (Figure 1) was designed and prepared using a dual UV lamp (85 cm in length) divided into coated and uncoated areas (ECOSET Co., Ltd., Ansan, Korea) connected to an electronic controller for 40 W/m$^2$. Fans at both ends were attached to minimize heat generation by the UV lamp. Intensities (μW/cm$^2$) of dual UV were measured at the site of petri dishes using a spectrometer (Jaz System; Ocean Optics, Inc., Petaluma, CA, USA) with software (Spectra Suite; Ocean Optics, Inc.). For UV inactivation, UV dose (mJ/cm$^2$) was calculated from multiplying the UV lamp intensity (μW/cm$^2$) by exposure time (s). Dual UV spectra were monitored from each side of the UV lamp.

## PXRD

MO nanoparticle crystallinities were analyzed via PXRD. The XRD patterns of the powdered nanoparticles were recorded from 20 to 80 2θ (degree, °) using a high resolution X-ray diffractometer (SmartLab, Rigaku Americas Co., Woodlands, TX, USA) with CuKα radiation. The data were collected and qualitatively analyzed in SmartLab. The average nanocrystal particle size was also calculated using Scherrer's equation:

$$\text{Particle size} = (K \times \lambda)/(\beta \times \cos\theta)$$

where K is a proportionality coefficient called shape factor (0.9), λ denotes the X-ray wavelength ($1.540\times10^{-10}$), β is the full width at half the maximum intensity in radians, and θ is the Bragg angle.[20]

## BET analysis

Specific surface area and pore analyses of MO nanoparticles were determined from nitrogen adsorption-desorption isotherms using a Qudrasorb SI (Quantachrome Instruments, Boynton Beach, FL, USA) with 1.0 h outgas at 300°C. Each sample was used at a range from 1.0 to 3.0 g. Experimental specific surface area, total pore volume, and average pore diameter were calculated using ASiQwin software (Quantachrome Instruments) based on BET theory. Theoretical specific surface area was also calculated using the following equation:

$$\text{Specific surface area} = 6/(D \times \rho)$$

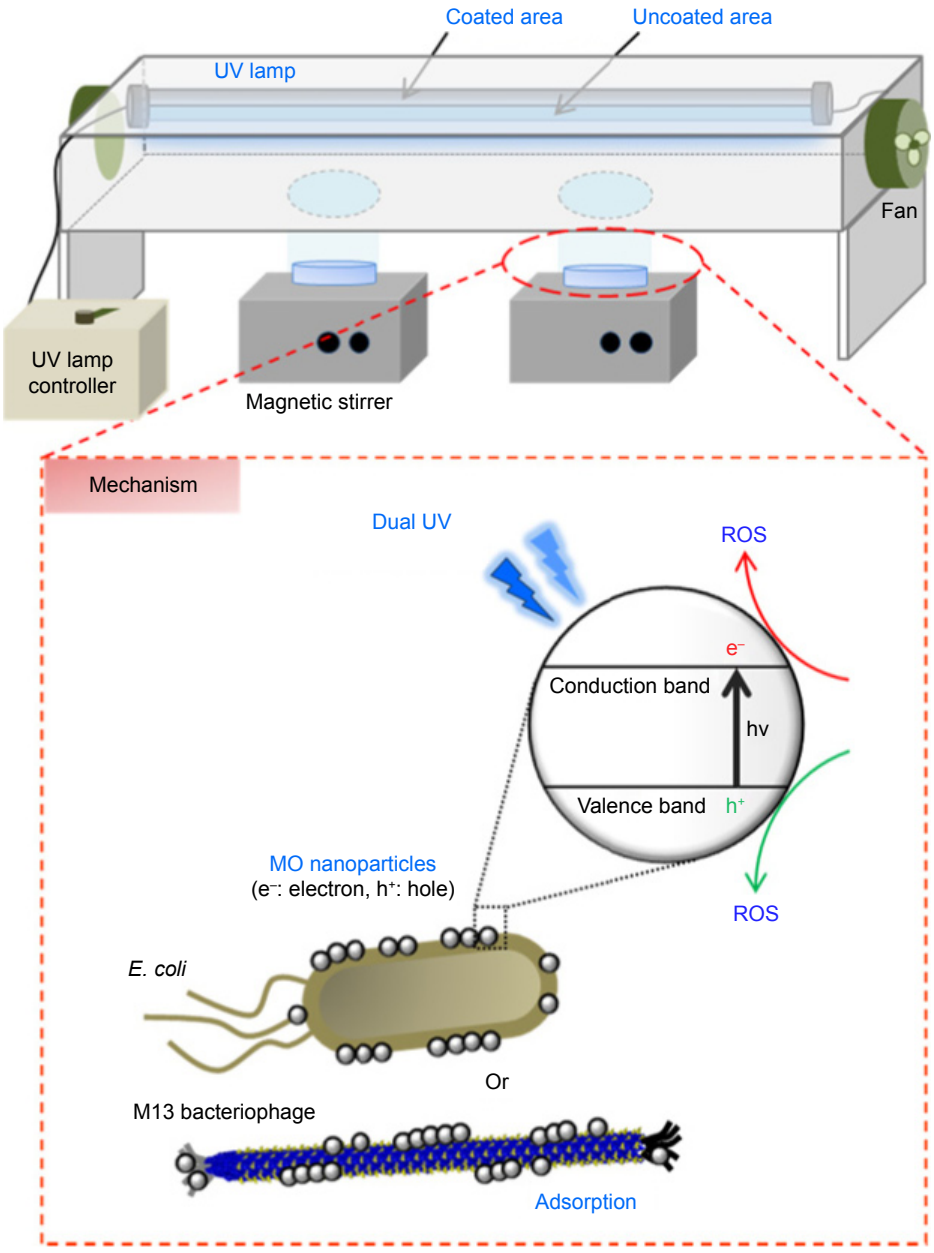


**Figure 1** Schematic diagram of dual UV-MO nanoparticle hybrid system using CBD and its antimicrobial mechanisms.
**Notes:** MO nanoparticles, dual UV (UV-A and UV-C), and dual UV-MO nanoparticle hybrid were applied to *Escherichia coli* and phage samples. UV-A and UV-C intensities were differentially controlled by lamp surface coating. MO nanoparticles showed intensive antimicrobial activity through microbial adsorption and ROS production by dual UV exposure.
**Abbreviations:** MO, metal oxide; CBD, collimated beam device; ROS, reactive oxygen species.

where D represents the particle size and ρ is the theoretical density (g/cm$^3$) of MO nanoparticles.[21] Theoretical density values of MO nanoparticles for ZnO, $ZnTiO_3$, MgO, and CuO were 5.61, 5.74, 3.58, and 6.31 g/cm$^3$, respectively.

## FE-SEM with EDS

MO nanoparticle morphologies were monitored using an FE-SEM (JSM-7100F; JEOL, Tokyo, Japan) operated at an acceleration voltage of 15.0 kV. Magnifications used were ×5,000 to ×50,000. EDS analysis was also performed at three points on the surface of MO nanoparticles to quantitatively determine the element compositions. Samples were investigated after platinum coating.

## AFM

The surface topology of MO nanoparticles was determined using an AFM (XE-100; Park Systems Inc., Santa Clara, CA, USA). MO nanoparticles were dispersed in water at 1.0 mg/mL.

After vortex mixing, samples were diluted with ethanol due to their poor dispersibility in water, and then dropped into silicon-based wafer and solvent was removed using a spin coater. After drying, AFM images were taken at a scanning area of 3×3 μm in a non-contact mode.

## EFM

EFM was conducted on an AFM (XE-100) in EFM mode accessorized with a AFM controller operating in a non-contact mode. MO nanoparticles with and without UV irradiation using each side of the UV lamp, coated and uncoated areas, were used as samples. UV exposure time was 10 s over three cycles (total 30 s for 30 min). EFM samples of MO nanoparticles were prepared as mentioned in the AFM section. Additionally, prior to image taking, silver paste was applied on each end of the silicon-based wafer to enhance the EFM image resolution. Scan size was 1×1 μm. In the lock-in amplifier, the measurement conditions of phase, frequency, and amplitude were 70°, 17 Hz, and 2 V, respectively. Sample bias was −1 V.

## Antimicrobial activity test

*E. coli* and phage were used as model microorganisms to confirm whether UV-MO nanoparticle hybrids had antimicrobial potentials as disinfection agents. MO nanoparticles and UV alone were used as controls. MO nanoparticles were dispersed in water at 1.0 mg/mL. In dark conditions, nanoparticles were added to *E. coli* ($10^4$ CFU) and incubated for 30 min. From samples, 1 mL was collected and added to LB/agar medium. The resultant samples were poured into plates and incubated in the dark at 37°C overnight. In the case of phages, $10^4$ PFU were used. Nanoparticles in water (1.0 mg/mL) were mixed with phages and incubated for 30 min. Then, 100 μL of samples were collected and incubated with overnight-cultured bacteria at room temperature for 60 min. After the top agars were mixed with those and poured onto LB/IPTG/Xgal plates, the plates were incubated at 37°C overnight for phage growth. For UV irradiation, UV was treated to MO nanoparticles for 30 s once or for 10 s in three cycles (total 30 s), while MO nanoparticles were incubated with *E. coli* or phage for 30 min. After UV irradiation, 1 mL of samples for *E. coli* was collected, added to LB/agar medium, and poured into plates. Then, plates were incubated in the dark at 37°C overnight. For phages, 100 μL of samples after UV irradiation were collected and incubated with overnight-cultured bacteria at room temperature for 60 min. Then, after the top agars were mixed with those samples and poured onto LB/IPTG/Xgal plates, the plates were incubated at 37°C overnight. Colonies and phage plaques were counted using ImageJ (NIH) after obtaining images.

## Statistical analysis

The results are expressed as the means ± SD. The statistical significance of the differences between groups was tested using the Student's *t*-test, with $p<0.05$ considered to be significant.

# Results

## Dual UV intensity and dose

Dual UV spectra were monitored and UV intensities of UV-A and UV-C were measured in the UV lamp. They showed a broad UV-A peak at 350~400 nm and a sharp UV-C peak at 253 nm (Figure S1). UV-C intensity in the uncoated area was 5.1-fold higher than that in the coated area (UV-C; uncoated >> coated), whereas UV-A intensity in the uncoated area was similar to that in the coated area of UV lamp (UV-A; uncoated ≈ coated). Table 1 shows the dual UV intensities of UV-A and UV-C based on UV irradiation areas of the lamp. In the coated area, UV-A and UV-C intensities were 495±13.8 μW/cm² and 94.4±35.7 μW/cm², respectively. However, in the uncoated area, UV-A and UV-C intensities were 447±92.7 μW/cm² and 478±27.8 μW/cm², respectively. Based on the dual UV intensities of UV-A and UV-C, the dose for a 10 s exposure was 4.95 mJ/cm² of UV-A and 0.944 mJ/cm² of UV-C in the coated area. The dual UV dose for 30 s exposure was 14.9 mJ/cm² of UV-A and 2.83 mJ/cm² of UV-C in the coated area. In the uncoated area, the UV dose for 10 s was 4.47 mJ/cm² of UV-A and 4.78 mJ/cm² of UV-C, and for 30 s was 13.4 mJ/cm² of UV-A and 14.3 mJ/cm² of UV-C, respectively.

## Crystallinity and average particle size of MO nanoparticles

The crystallinities of MO nanoparticles were confirmed using the diffraction patterns in the range of 20~80 2θ (degree, °) (Figure 2). MO nanoparticles showed sharp crystalline peaks. The PXRD patterns of ZnO (Figure 2A), $ZnTiO_3$ (Figure 2B), MgO (Figure 2C), and CuO (Figure 2D) nanoparticles were matched to those of pure MO after

**Table 1** Dual UV intensities of UV-A and UV-C in the UV lamp

| UV irradiation site | UV intensity (μW/cm²) | |
|---|---|---|
| | UV-A | UV-C |
| Coated area | 495±13.8 | 94.4±35.7 |
| Uncoated area | 447±92.7 | 478±27.8 |

**Note:** Data presented as mean ± standard deviation (n=3).

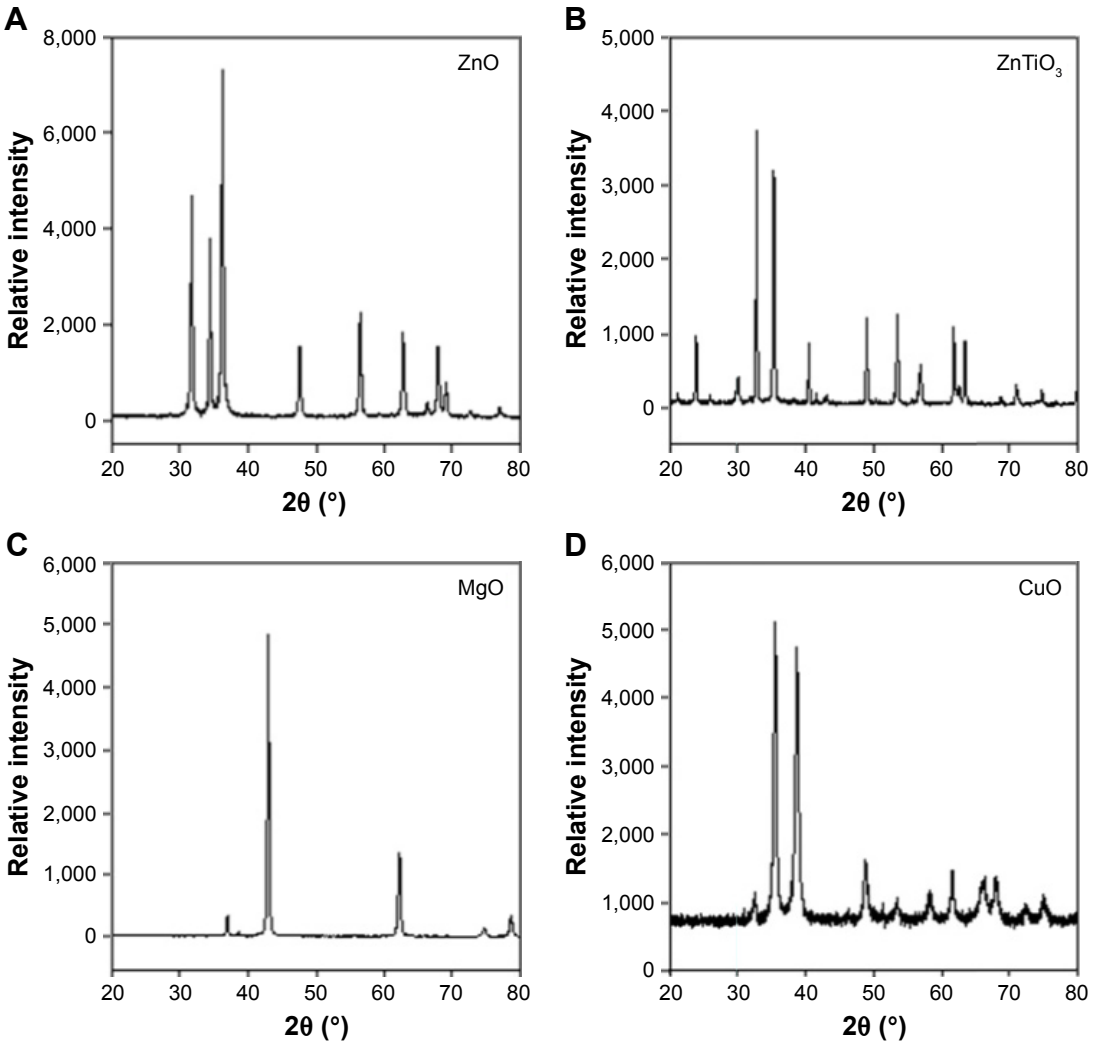


**Figure 2** X-ray diffractograms of MO nanoparticles.
**Note:** (**A**) ZnO, (**B**) $ZnTiO_3$, (**C**) MgO, and (**D**) CuO.
**Abbreviation:** MO, metal oxide.

qualitative analysis (reference database card no ICDD-01-076-0704 for ZnO, ICDD-00-015-0591 and ICDD-00-039-0190 for $ZnTiO_3$, ICDD-00-045-0946 for MgO, and ICDD-01-089-5898 for CuO). Upon calculating the average sizes of MO nanoparticles followed by Scherrer's equation, ZnO, $ZnTiO_3$, MgO, and CuO nanoparticle sizes were 33 nm, 49 nm, 31 nm, and 18 nm, respectively.

## Specific surface area and pore characterization

Table 2 lists the surface characteristics of specific surface area, pore volume, and pore size in MO nanoparticles following BET analysis. ZnO nanoparticles had a large specific surface area of 25.6 $m^2/g$ compared to other nanoparticles (ZnO >> $ZnTiO_3$ > MgO >> CuO). Theoretically calculated values of specific surface areas were 32, 21, 53, and 54 $m^2/g$ for ZnO, $ZnTiO_3$, MgO, and CuO nanoparticles, respectively. Their experimental values were less than theoretical values, suggesting the generation of clusters and aggregates. For the pore volume of nanoparticles, $ZnTiO_3$ nanoparticles showed the largest pore volume of 0.86 cc/g ($ZnTiO_3$ >> MgO > ZnO >> CuO). $ZnTiO_3$ nanoparticles also had the largest

**Table 2** Surface characteristics of MO nanoparticles

| Nanoparticles | Theoretical specific surface area ($m^2/g$) | Specific surface area ($m^2/g$) | Pore volume (cc/g) | Pore size (nm) |
|---|---|---|---|---|
| ZnO | 32 | 25.58 | 0.1404 | 21.95 |
| $ZnTiO_3$ | 21 | 13.20 | 0.8638 | 261.8 |
| MgO | 53 | 15.44 | 0.1922 | 49.80 |
| CuO | 54 | 8.620 | 0.04931 | 22.88 |

**Abbreviation:** MO, metal oxide.

pore size of 261.8 nm ($ZnTiO_3$ >> MgO > CuO > ZnO). However, the pore sizes of ZnO, MgO, and CuO nanoparticles were less than 100 nm, in the range of 21.95 to 49.80 nm.

## Morphology and size of MO nanoparticles

MO nanoparticles had an irregular shape which was a relatively spherical (Figure 3A–C) or flower-like shape (Figure 3D) with nanoparticle sizes less than 100 nm in diameter. They showed uniform size distribution, but the nanoparticles were self-adsorptive, thereby generating clusters. In a hydrodynamic environment, MO nanoparticles formed large aggregates over 100.0 µm due to their poor dispersibility although their primary particle sizes were within the nanoscale range (Figure S2).

## Atomic composition of MO nanoparticles

MO nanoparticles had atomic elements proportional to their chemical formula based on the EDS results (Table 3). ZnO nanoparticles consisted of 49% Zn, 47% O, and 4% Al suggesting Al was used as dopant in ZnO nanoparticles. $ZnTiO_3$ nanoparticles showed 21% Zn, 19% Ti, and 60% O. MgO nanoparticles had 50% Mg and 50% O. CuO nanoparticles had 44% Cu and 56% O.

## Surface topology of MO nanoparticles

Figure 4 shows the topologies and 3D structures of MO nanoparticles. MO nanoparticles showed a ball-shaped multifaceted O-terminated surface of nanocrystalline structures based on the measurement of small forces between the AFM tip and the surface of MO nanoparticles. In MO nanoparticles, the combination of chemical forces, van der Waals forces, and electrostatic forces was utilized to investigate the superposition of the surface and the chemical geometric structures. The diameters of all MO nanoparticles were less than 100 nm.

## Electrostatic characteristics of MO nanoparticles

We confirmed the electrostatic properties of MO nanoparticles before and after dual UV irradiation (Figure 5).

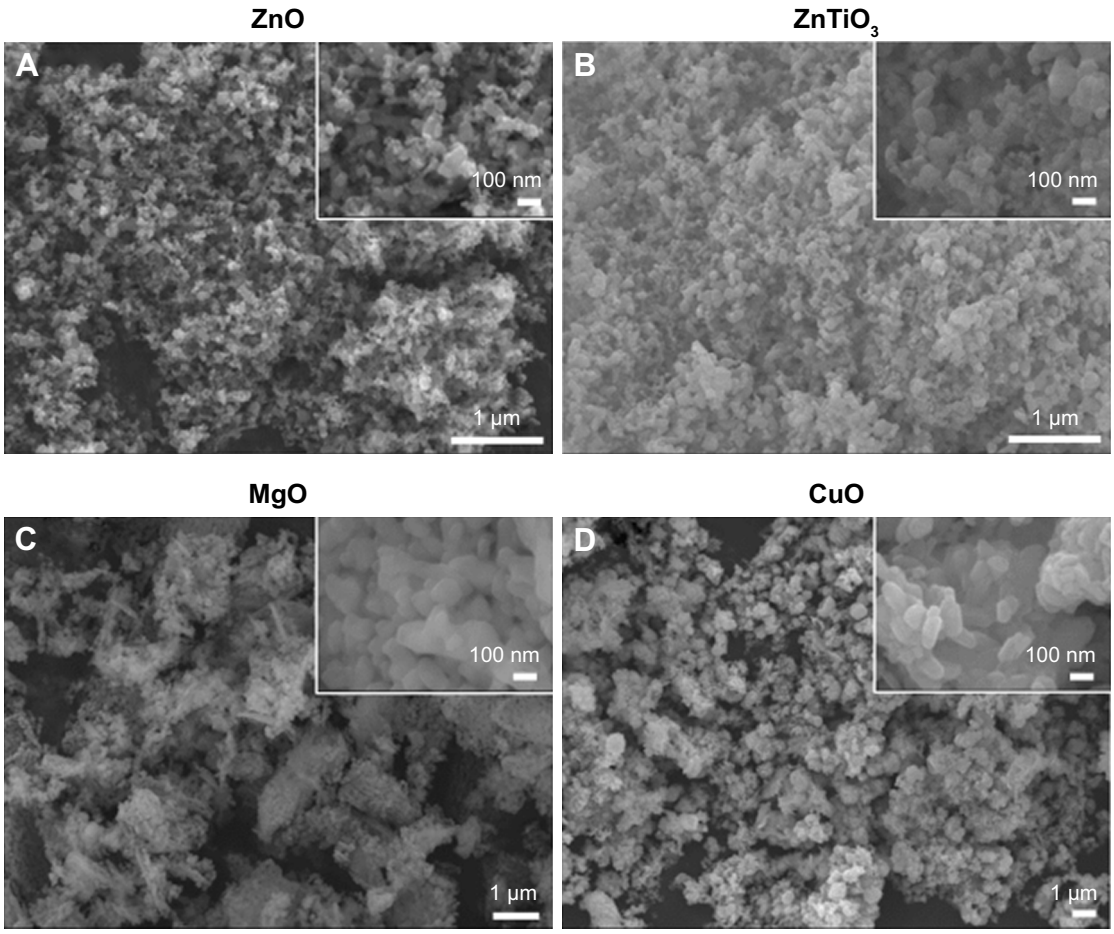


**Figure 3** FE-SEM images of MO nanoparticles.
**Note:** (**A**) ZnO, (**B**) $ZnTiO_3$, (**C**) MgO, and (**D**) CuO.
**Abbreviations:** FE-SEM, field emission-scanning electron microscopy; MO, metal oxide.

**Table 3** Atomic compositions of MO nanoparticles

| Nanoparticles | Atomic compositions (%) | | | | | |
|---|---|---|---|---|---|---|
| | Zn | Al | Ti | Mg | Cu | O |
| ZnO | 49.2±2.7 | 3.5±0.3 | | | | 47.4±2.9 |
| $ZnTiO_3$ | 21.4±0.5 | | 19.1±4.2 | | | 59.5±3.6 |
| MgO | | | | 50.4±1.7 | | 49.6±1.7 |
| CuO | | | | | 43.6±0.7 | 56.4±0.7 |

**Note:** Data presented as mean ± standard deviation (n=3).
**Abbreviation:** MO, metal oxide.

For dual UV irradiation, the intensities of UV-A and UV-C were controlled using the coated and uncoated areas of the UV lamp. Three cyclic exposures of 10 s for 30 min were used.

## Electrostatic characteristics: MO nanoparticles without UV irradiation

Figure 5A–D shows the EFM images of MO nanoparticles in the dark condition to monitor the electrostatic properties. ZnO nanoparticles generated clusters and showed 1.4~1.7 V of amplitude (Figure 5A). $ZnTiO_3$ and MgO nanoparticles had 1.8~2.0 V (Figure 5B) and 1.1~1.3 V of amplitude (Figure 5C), respectively. CuO nanoparticles particularly had 3.0~3.4 V of amplitude (Figure 5D). For the analyses of absolute surface amplitude and potential, scanning Kelvin probe microscopy (SKPM) images of ZnO and $ZnTiO_3$ nanoparticles were obtained (Figure S3A and B). ZnO nanoparticle aggregates showed 28.2~48.8 mV of amplitude and −1.5~−1.4 V of surface potential (Figure S3A). $ZnTiO_3$ nanoparticles showed 31.8~43.8 mV of amplitude and −1.7~−1.6 V of surface potential (Figure S3B).

## Electrostatic characteristics: MO nanoparticles after dual UV irradiation

EFM images of MO nanoparticles after dual UV irradiation are shown in Figure 5E–H by coated area and in Figure 5I–L by uncoated area. After dual UV irradiation from the coated area, the amplitudes of MO nanoparticles are changed without topological changes. From the coated area, ZnO nanoparticles showed 2.3~2.7 V of amplitude (Figure 5E). $ZnTiO_3$ and MgO nanoparticles had 1.6~1.8 V (Figure 5F) and 450~650 mV of amplitude (Figure 5G), respectively. CuO nanoparticles particularly had 2.1~2.3 V of amplitude (Figure 5H). For the uncoated area, ZnO nanoparticles showed 2.25~3.25 V of amplitude (Figure 5I). $ZnTiO_3$ and MgO nanoparticles had 1.9~2.2 V (Figure 5J) and 680~840 mV of amplitude (Figure 5K), respectively. CuO nanoparticles particularly had 1.8~2.1 V of amplitude (Figure 5L). In SKPM images, after UV irradiation from a coated area, the amplitude and potential of ZnO nanoparticles were 22.2~32.3 mV and −0.99~−0.93 V (Figure S3C). However, $ZnTiO_3$ nanoparticles changed from 31.8~43.8 mV of amplitude and −1.7~−1.6 V of potential to 19.2~27.5 mV of amplitude and −414.4~−369.3 mV of potential after UV irradiation using the coated area (Figure S3D). Using an uncoated area in the UV lamp, ZnO nanoparticles had 46.1~73.5 mV of amplitude and −2.2~−2.1 V of potential (Figure S3E), whereas $ZnTiO_3$ nanoparticles showed 39.7~48.2 mV of amplitude and −1.40~−1.37 V of potential (Figure S3F). Additionally, upon monitoring the electromechanical properties, d33 (pm/V) of ZnO nanoparticles from the piezoelectric force microscopy results showed no significant difference after dual UV irradiation with three cyclic exposures, suggesting the piezoelectrically free electrostatic response of ZnO nanoparticles (Figure S4).

## Antimicrobial activity

Based on the physicochemical and electrostatic properties of MO nanoparticles before and after dual UV irradiation, the antimicrobial effects of UV-MO nanoparticle hybrid system on *E. coli* and phage were evaluated after single and cyclic exposures of dual UV. MO nanoparticles and UV irradiation alone were used as controls.

## Antimicrobial activity: antibacterial effects on *E. coli*

The antibacterial effects of dual UV-MO nanoparticle hybrids on *E. coli* were estimated. Figure 6 shows the concentration of MO nanoparticles versus Log(CFU) profiles after single or cyclic UV exposure (Figure 6A), and the representative plate images of colonies (Figure 6B–G). All MO nanoparticles at 1.0 mg/mL, except $ZnTiO_3$, showed antibacterial effects on *E. coli*. In MO nanoparticles, ZnO nanoparticles showed the highest antibacterial potential against *E. coli* after 30 min exposure (ZnO > MgO > CuO >> $ZnTiO_3$). Toxicity from MO nanoparticles was mediated by adsorption potential from surface characteristics and release of metal ions from MO nanoparticles, even though it was not perfectly matched due to their complexity. Release of Zn ion from ZnO nanoparticles in water was less than 1 ppm (Figure S5). Mg ion showed the highest release level in water after 7-day incubation. However, Zn, Ti, and Cu ions were only minimally released from $ZnTiO_3$ and CuO nanoparticles. Under dual UV irradiation using the uncoated lamp area, $ZnTiO_3$ and MgO nanoparticles showed enhanced antibacterial activity against *E. coli* (Figure 6A). In addition, cyclic exposures from the uncoated UV bulb area with MO nanoparticles showed a superior antibacterial effect against *E. coli* (Figure 6E and F). No colonies of *E. coli* were detected after MgO nanoparticle treatments under dual UV irradiation except a 30 s treatment

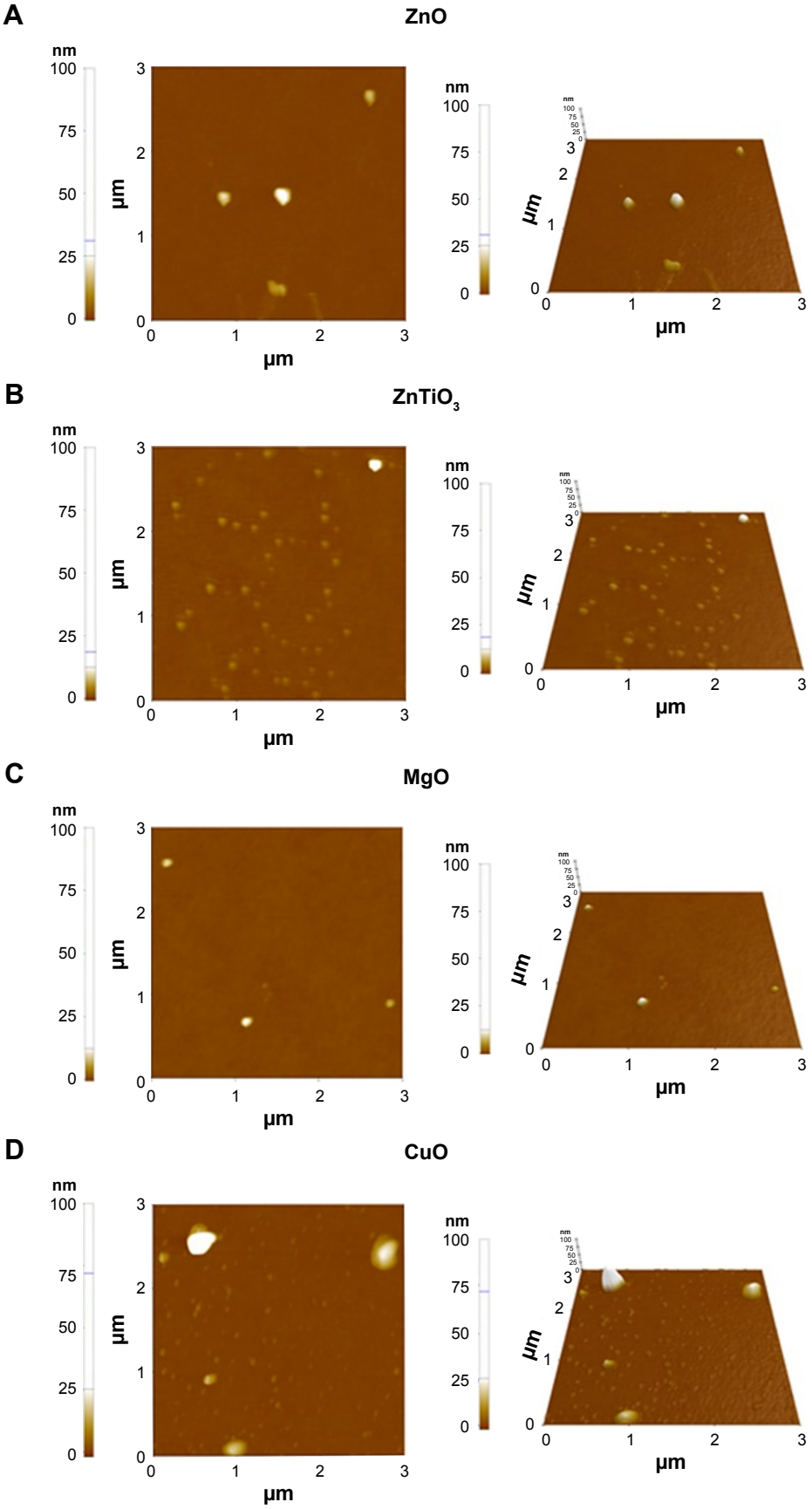


**Figure 4** AFM images of MO nanoparticles.
**Notes:** (**A**) ZnO, (**B**) $ZnTiO_3$, (**C**) MgO, and (**D**) CuO. 2D and 3D images of AFM were listed.
**Abbreviations:** AFM, atomic force microscopy; MO, metal oxide.

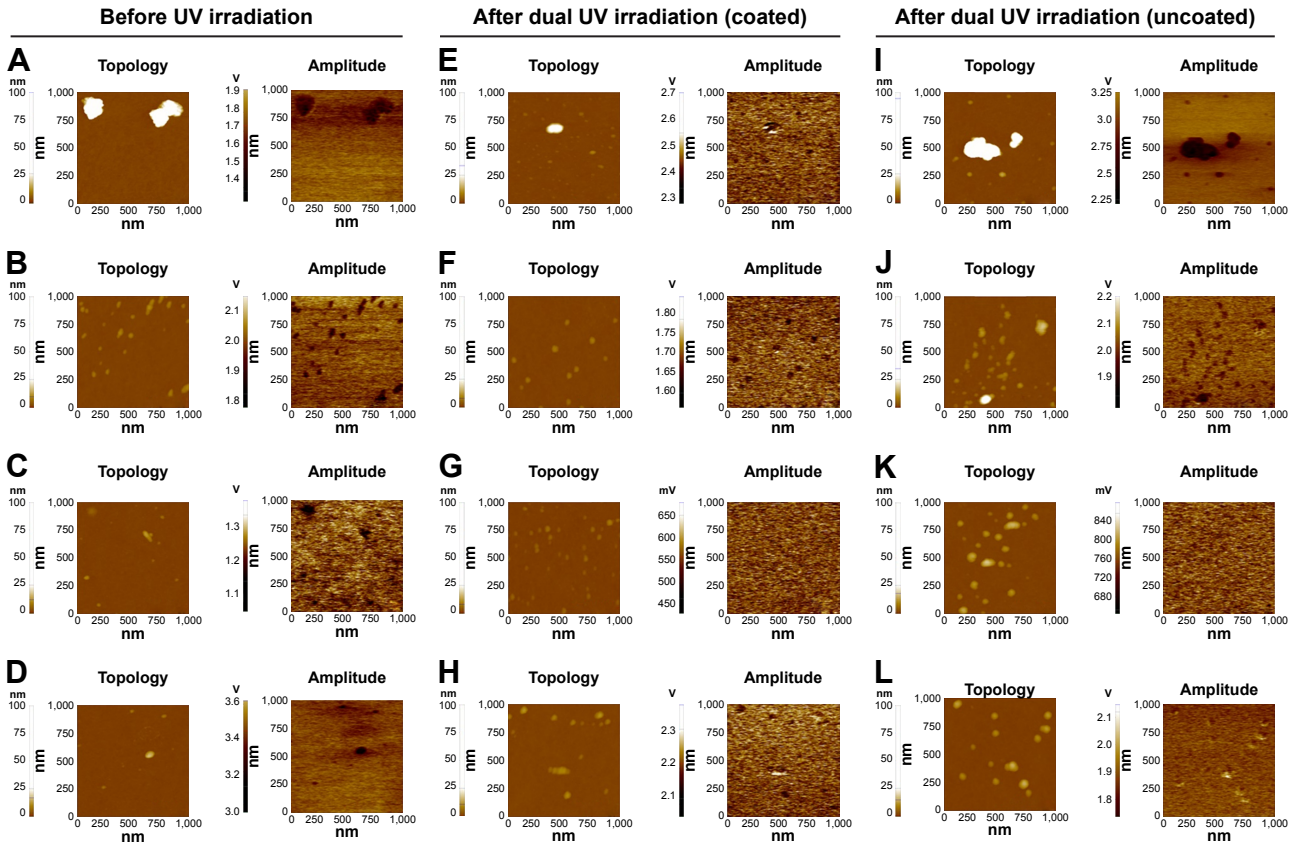


**Figure 5** EFM images of MO nanoparticles before/after dual UV irradiation.
**Notes:** MO nanoparticles before UV irradiation: (**A**) ZnO, (**B**) $ZnTiO_3$, (**C**) MgO, and (**D**) CuO. MO nanoparticles after cyclic UV exposure using the coated area: (**E**) ZnO, (**F**) $ZnTiO_3$, (**G**) MgO, and (**H**) CuO. MO nanoparticles after cyclic UV exposure using the uncoated area: (**I**) ZnO, (**J**) $ZnTiO_3$, (**K**) MgO, and (**L**) CuO. MO nanoparticles were exposed to dual UV of UV-A and UV-C for 10 s over three cycles for 30 min. Topologies and amplitudes of MO nanoparticles were presented.
**Abbreviations:** EFM, electrostatic force microscopy; MO, metal oxide.

from a coated area. However, in the plates after cyclic UV exposures of the uncoated area with ZnO nanoparticles, colonies were still detected. In the case of CuO nanoparticles, no colonies were detected after CuO nanoparticle treatment (1.0 mg/mL) under dual UV irradiation with single and cyclic exposures from the coated area as well as the uncoated area. Even with 0.1 mg/mL of CuO nanoparticles, and dual UV single exposure irradiation from an uncoated area for 10 s, colonies were not detected (Figure S6).

## Antimicrobial activity: inactivation effects on phages

The inactivation effects of dual UV-MO nanoparticles on phages were monitored. Figure 7 shows the concentration of MO nanoparticles versus Log(PFU) profiles after single or cyclic UV exposure (Figure 7A), and representative plaque plate images (Figure 7B–G). In all MO-treated plates, except ZnO nanoparticles, plaques were not detected after cyclic dual UV exposure from the uncoated area of the UV bulb. Specifically, CuO nanoparticles even at 0.1 mg/mL, were associated with no plaques after dual UV irradiation from the uncoated area after a single 30 s dose or three cyclic 10 s doses (Figure S6). However, none of the MO nanoparticles demonstrated inactivation effects on phages in the absence of UV irradiation.

# Discussion

Here we report the antimicrobial activities of a dual UV-MO nanoparticle hybrid system on *E. coli* and phages after a short exposure to dual UV (30 s or 10 s in three cycles) and MO nanoparticles (30 min) (Figure 1). ZnO, $ZnTiO_3$, MgO, and CuO nanoparticles were used in the hybrid system to screen for superior antimicrobial activities. The physicochemical properties of MO nanoparticles (e.g., size, crystallinity, surface characteristics, morphology, and electrostatic characterization) were evaluated due to their interaction with microorganisms. UV-A and UV-C as a dual UV were used in the CBD to evaluate their disinfection potential against *E. coli* and phages. A CBD was developed to collect the UV beam and to calculate UV dose under dual UV irradiation.

Dual UV exposure with UV-A and UV-C is a cutting edge technique. Each spectrum of UV-A and UV-C is a powerful

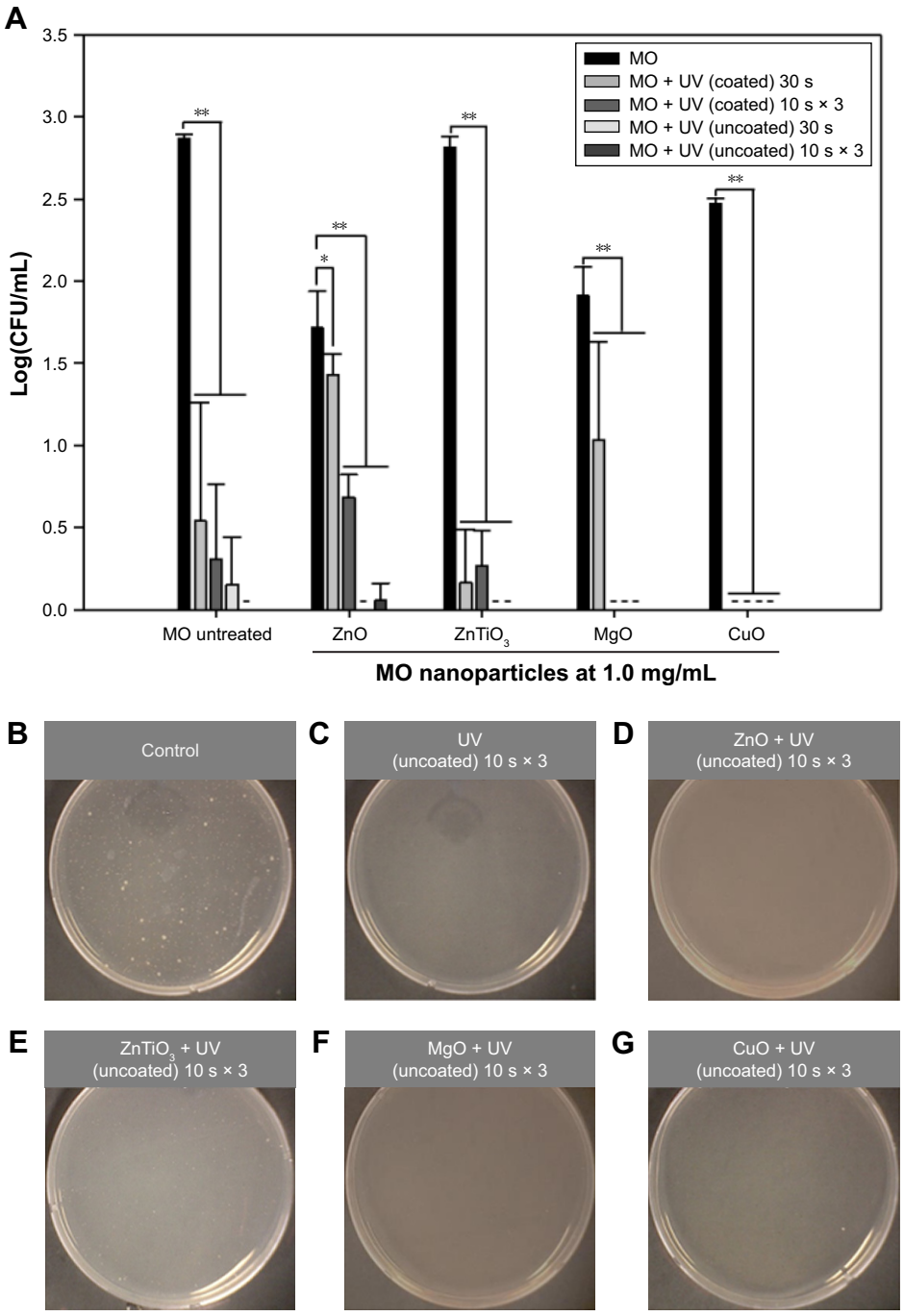


**Figure 6** Antibacterial effects of dual UV-MO nanoparticles hybrid on *Escherichia coli.*
**Notes:** (**A**) The plot of Log(CFU/mL) versus MO nanoparticle. Dual UV was exposed for 30 s or 10 s in three cycles, while MO nanoparticles at 1.0 mg/mL were treated for 30 min. Representative plate images of colonies after the treatment of cyclic exposure (10 s × 3) from the uncoated area and MO nanoparticles are shown: (**B**) control (untreated), (**C**) UV (uncoated), (**D**) ZnO, (**E**) $ZnTiO_3$, (**F**) MgO, and (**G**) CuO. -, not detected; *$p<0.05$; **$p<0.01$.
**Abbreviation:** MO, metal oxide.

disinfection tool.[5,15,22] UV-C has a germicidal peak at 253 nm and is generally used for disinfection. UV-A also has disinfection potential against harmful insects. In the hybrid system, differential intensities of UV-A and UV-C in dual UV (Table 1; Figure S1) were detected in the CBD. UV-C was partially blocked by coating the half-sided surface of the UV lamp compared to UV-A. UV-C intensities in the coated areas of the UV lamp were lower than those in uncoated areas of the UV lamp, whereas UV-A intensities were maintained in both areas of the UV lamp.

MO nanoparticles are innovative materials used as nano-antibiotics and disinfection agents in biomedical

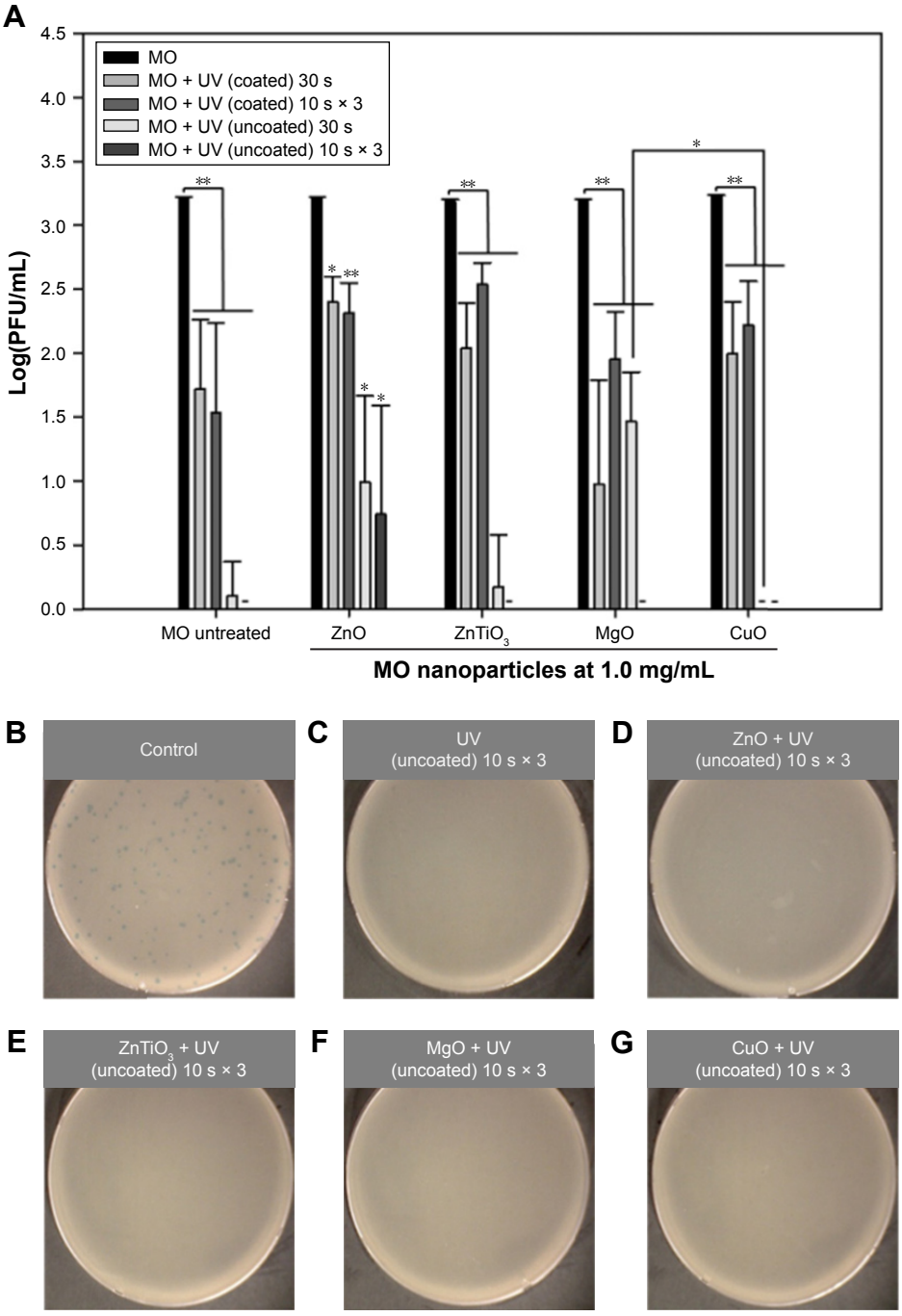


**Figure 7** Inactivation effects of dual UV-MO nanoparticle hybrid on phages.
**Notes:** (**A**) The plot of Log(PFU/mL) versus MO nanoparticles. MO nanoparticles at 1.0 mg/mL were treated for 30 min with and without dual UV irradiation for 30 s or 10 s in three cycles. After treatment of cyclic exposure (10 s × 3) from the uncoated area and MO nanoparticles, representative plate images of plaques are shown: (**B**) control (untreated), (**C**) UV (uncoated), (**D**) ZnO, (**E**) $ZnTiO_3$, (**F**) MgO, and (**G**) CuO. -, not detected; *$p<0.05$; **$p<0.01$.
**Abbreviation:** MO, metal oxide.

applications,[1,14] among their wide uses as catalysts, sensors, batteries, capacitors, cosmetics, and pharmaceuticals.[23,24] They have antimicrobial activities against various bacteria and viruses, such as *Streptococcus aureus* (Gram-positive), *E. coli* (Gram-negative), and MS2 bacteriophages,[5,25,26] and even antibiotic-resistant bacteria[1,27] due to their adsorption to biomembrane and photocatalytic functions. They possibly enhance adsorption potential in terms of interaction with membrane components such as proteins, lipids, and peptides.[25] Their adsorption intensities were differentially expressed depending on the types of MO nanoparticles, and microorganism membrane components. Under UV and light

irradiation, MO nanoparticles as photocatalysts generated ROS and caused toxicities in microorganisms.

The physicochemical properties of MO nanoparticles affect antimicrobial activities due to their interaction with microorganisms.[8,28] MO nanoparticles generally have a highly crystalline structure, uniform particle shape, nanoscale size, and large surface area with mesopores for chemical and biological adsorption.[7,10] These properties were dependent on the synthesis techniques (e.g., sol-gel processing[11] and thermal evaporation[29]) and the conditions which affect MO nanocrystal growth.[30] From the sharp peaks in PXRD patterns (Figure 2), ZnO nanoparticles showed a hexagonal Wurzite structure. $ZnTiO_3$ and MgO nanoparticles had a stable hexagonal structure[31] and a cubic structure,[32] respectively. CuO nanoparticles showed a monoclinic phase structure.[33,34] MO nanoparticles showed sizes less than 100 nm in diameter (Figure 3). However, their hydrodynamic sizes were over 100.0 µm due to their aggregate formation in water (Figure S2), which is comparable to the results from Zhang et al.[35] MO nanoparticles also had a large surface area with mesopores (Table 2), suggesting high adsorption properties with respect to biological membranes which led to membrane rupture, blebs, clumps, and cell leakages.[25] The oxidation states were confirmed via elemental analysis of the MO nanoparticles (Table 3). MO nanoparticles were considered as pure materials without further acid digestion.[36]

The surface topologies and electrostatic properties are considered as critical factors when monitoring antimicrobial activities of MO nanoparticles with and without dual UV irradiation based on biomembrane adsorption and ROS generation.[28,35,37,38] The nanocrystalline structures of MO nanoparticles (Figure 4) were matched with PXRD and FE-SEM results. In terms of electrostatic characteristics, MO nanoparticles function as photocatalysts that lead to antimicrobial activities[10,22] based on ROS generation by the electronic curvatures in reciprocal space of the conduction band minimum and valence band maximum, and dispersions of electron-hole effective masses.[24] They have wide band gap energies (ZnO, 3.3 eV; $ZnTiO_3$, 2.9 eV; MgO, 7.8 eV; CuO, 1.2 eV). Upon energy elevation over the band gap energies of MO nanoparticles during UV irradiation, MO nanoparticles generate ROS, such as hydroxyl radical and singlet oxygen in hydrodynamic environments.[22,35] Energy application promotes electron transfer from photodynamic water splitting to geochemical cycling of elements in the interfaces of MO nanoparticles and water.[24,39,40] MO nanoparticles showed stable electronic properties in EFM images before (Figure 5A–D) and after dual UV irradiation using coated (Figure 5E–H) and uncoated areas (Figure 5I–L) in the hybrid system. This result was confirmed by SKPM (Figure S3). A piezoelectrically-free electrostatic response was observed in ZnO nanoparticles after dual UV irradiation (Figure S4). However, the band gap energy variations seen could be caused by defects, crystal structure, and temperature of MO nanoparticles.[41,42] Photoexcitation responses can also be confirmed using UV and Fourier transform-infrared spectroscopy (FT-IR).[43]

The dual UV-MO nanoparticle hybrid system can be applied for the disinfection of bacteria and viruses. *E. coli* and phages were used as model microorganisms. The antimicrobial activities of dual UV-MO nanoparticle hybrids on *E. coli* (Figure 6) and phages (Figure 7) were evaluated after single or cyclic UV exposure. MO nanoparticles at 1.0 mg/mL showed antimicrobial activity against *E. coli* in the dark condition even after a short exposure of 30 min, except for $ZnTiO_3$ nanoparticles (Figure 6A). Among MO nanoparticles not combined with UV treatment, ZnO nanoparticles showed the highest activities based on their high adsorption capacity for microorganism biomembrane due to their large specific surface area (ZnO > $ZnTiO_3$ > MgO > CuO), and their metal ion release at the ppb level (Figure S5).[26] Under dual UV irradiation, MgO nanoparticles applied at cyclic exposure and CuO nanoparticles at single and cyclic exposures completely removed *E. coli* colonies, although UV-C intensities decreased at the coated area (Figures 6A and S6). On the other hand, MO nanoparticles did not have phage-inactivation activities, but dual UV irradiation was essential to inactivate phage activity during treatment with MO nanoparticles (Figure 7A). Based on the electrostatic properties of MO nanoparticles as photocatalysts, the dual UV-MO nanoparticle hybrid system enhanced activities against phages as well as *E. coli* compared to MO nanoparticles or UV alone (Figure 7A–G). Specifically, cyclic dual UV treatment at high UV-C intensity (uncoated area) showed superior antimicrobial effects against phages, as well as *E. coli*, compared to single exposures with dual UV at low UV-C intensity (coated area). These results suggested that UV-C intensities drove the antimicrobial effects. However, when using the uncoated area of the UV lamp, colonies and plaques were still detected after treatment with dual UV-ZnO nanoparticles at 1.0 mg/mL, suggesting hindrance of the dual UV/ZnO nanoparticle/microorganism interaction in a hydrodynamic environment.

The mechanisms of antimicrobial activities from dual UV-MO (ZnO, $ZnTiO_3$, MgO, and CuO) nanoparticle hybrid systems are not fully understood due to their complexity, but there are many hypotheses, including:[25,26,28] 1) adsorption,

2) ROS generation, 3) ion release, 4) cell wall damage, and 5) penetration of MO nanoparticles into the cell envelope. Adsorption and ROS generation mainly explained the induction of antimicrobial activities in the dual UV-MO nanoparticle hybrid system.[44] The antimicrobial potential of the hybrid system is based on the physicochemical properties of MO nanoparticles and the interaction between MO nanoparticles and UV irradiation, or MO nanoparticles and microorganisms.[25,44] Specifically, the adsorption of ZnO nanoparticles to *E. coli* was previously reported based on the interaction between nanoparticles and *E. coli* lipopolysaccharides, which vary according to the types of MO nanoparticles mentioned previously.[25] In the case of MgO nanoparticles, they do not induce lipid peroxidation in microbial biomembranes by ROS production, but a metabolic reduction occurs.[44] CuO nanoparticles additionally function to inhibit metabolic proteins and DNA in bacteria and viruses.[44]

Overall, the dual UV-MO nanoparticle hybrids of CuO nanoparticles could be successfully applied in industry as photocatalysts, because cleaning and sanitization are tightly regulated in the pharmaceutical and water purification industries to prevent microbial contamination.[45] In the industrial good manufacturing practice for pharmaceutical manufacturing, sanitizers should have a 3 Log CFU reduction. Specifically, microbial contamination should be prevented in various types of water (e.g., drinking water, water for injection, and sterile purified water). Under dual UV irradiation in our hybrid system, CuO nanoparticles showed significant disinfection potentials for both bacteria and viruses, more so than MO nanoparticles or UV alone even at 0.1 mg/mL for 30 s or 10 s in three cycles of high UV-C exposure from dual UV exposure (using the uncoated lamp area) (Figure S6). Hassana et al reported the minimum inhibitory concentration/minimum bactericidal concentration value for CuO nanoparticles as 2.5 μg/mL after 20 h of incubation with *E. coli*;[46] Gopinath et al confirmed the antimicrobial potential of CuO nanoparticles using confocal microscopy.[34] Promisingly, compared to Hassana et al, the dual UV-CuO nanoparticle hybrid system could be extended to short time exposure-based disinfection even at 0.1 mg/mL of CuO nanoparticles.

## Conclusion

$ZnO$, $ZnTiO_3$, MgO, and CuO nanoparticles hybridized with a dual UV irradiation system of UV-A and UV-C demonstrated enhanced antimicrobial activities against *E. coli* and phages in water. The physicochemical and electrostatic properties of MO nanoparticles were confirmed. Cyclic UV irradiation was valuable for disinfection compared with single UV exposure in the hybrid system. These results suggest dual UV irradiated MO nanoparticles can be used as disinfection agents in water, as they have demonstrated antimicrobial activities against *E. coli* and phages. Dual UV-MO nanoparticle hybrid system has promising potential to be applied for future disinfection systems.

## Acknowledgments

This work was supported by the Korea Ministry of Environment (MOE) as part of the, "The advancement of scientific research and technological development in environmental science program (2016000140006)." We thank the operators in YCRF of Yonsei University for microscopic analysis.

## Disclosure

The authors report no conflicts of interest in this work.

## References

1. Huh AJ, Kwon YJ. "Nanoantibiotics": a new paradigm for treating infectious diseases using nanomaterials in the antibiotics resistant era. *J Control Release*. 2011;156(2):128–145.
2. Pelgrift RY, Friedman AJ. Nanotechnology as a therapeutic tool to combat microbial resistance. *Adv Drug Deliv Rev*. 2013;65(13–14):1803–1815.
3. Dizaj SM, Lotfipour F, Barzegar-Jalali M, Zarrintan MH, Adibkia K. Antimicrobial activity of the metals and metal oxide nanoparticles. *Mater Sci Eng C Mater Biol Appl*. 2014;44:278–284.
4. Cutler TD, Zimmerman JJ. Ultraviolet irradiation and the mechanisms underlying its inactivation of infectious agents. *Anim Health Res Rev*. 2011;12(1):15–23.
5. Beck SE, Rodriguez RA, Hawkins MA, Hargy TM, Larason TC, Linden KG. Comparison of UV-Induced Inactivation and RNA Damage in MS2 Phage across the Germicidal UV Spectrum. *Appl Environ Microbiol*. 2015;82(5):1468–1474.
6. Pablos C, Marugan J, van Grieken R, Serrano E. Emerging micropollutant oxidation during disinfection processes using UV-C, UV-C/$H_2O_2$, UV-A/$TiO_2$ and UV-A/$TiO_2$/$H_2O_2$. *Water Res*. 2013;47(3):1237–1245.
7. Fu PP, Xia Q, Hwang HM, Ray PC, Yu H. Mechanisms of nanotoxicity: generation of reactive oxygen species. *J Food Drug Anal*. 2014;22(1):64–75.
8. Kasemo B, Lausmaa J. Material-tissue interfaces: the role of surface properties and processes. *Environ Health Perspect*. 1994;102(Suppl 5):41–45.
9. Melchionna M, Prato M, Fornasiero P. Mix and match metal oxides and nanocarbons for new photocatalytic frontiers. *Catal Today*. 2016;277:202–213.
10. Picone A, Riva M, Brambilla A, et al. Reactive metal-oxide interfaces: A microscopic view. *Sci Rep*. 2016;71(1):32–76.
11. Meenakshi G, Sivasamy A. Synthesis and characterization of zinc oxide nanorods and its photocatalytic activities towards degradation of 2,4-D. *Ecotoxicol Environ Saf*. 2017;135:243–251.
12. Das S, Srivastava VC. Microfluidic-based photocatalytic microreactor for environmental application: a review of fabrication substrates and techniques, and operating parameters. *Photochem Photobiol Sci*. 2016;15(6):714–730.
13. Horie M, Fujita K, Kato H, et al. Association of the physical and chemical properties and the cytotoxicity of metal oxide nanoparticles: metal ion release, adsorption ability and specific surface area. *Metallomics*. 2012;4(4):350–360.

14. Lemire JA, Harrison JJ, Turner RJ. Antimicrobial activity of metals: mechanisms, molecular targets and applications. *Nature Reviews Microbiology*. 2013;11:371–384.
15. Shen C, Turney TW, Piva TJ, Feltis BN, Wright PF. Comparison of UVA-induced ROS and sunscreen nanoparticle-generated ROS in human immune cells. *Photochem Photobiol Sci*. 2014;13(5):781–788.
16. Pal A, Alam S, Mittal S, et al. UVB irradiation-enhanced zinc oxide nanoparticles-induced DNA damage and cell death in mouse skin. *Mutat Res Genet Toxicol Environ Mutagen*. 2016;807:15–24.
17. Ali A, Rashid MA, Huang QY, Lei CL. Influence of UV-A radiation on oxidative stress and antioxidant enzymes in Mythimna separata (Lepidoptera: Noctuidae). *Environ Sci Pollut Res Int*. 2017;24(9):8392–8398.
18. Dai T, Vrahas MS, Murray CK, Hamblin MR. Ultraviolet C irradiation: an alternative antimicrobial approach to localized infections? *Expert Rev Anti Infect Ther*. 2012;10(2):185–195.
19. Ali A, Rashid MA, Huang QY, Lei CL. Effect of UV-A radiation as an environmental stress on the development, longevity, and reproduction of the oriental armyworm, Mythimna separata (Lepidoptera: Noctuidae). *Environ Sci Pollut Res Int*. 2016;23(17):17002–17007.
20. Langford JI, Wilson AJ. Scherrer after sixty years: A survey and some new results in the determination of crystallite size. *J Appl Crystallogr*. 1978;11:102–113.
21. Hjiri M, Mir L, Leonardi S. Synthesis, Characterization and sensing properties of AZO and IZO nanomaterials. *Chemosensors*. 2014;2(2):121–130.
22. Li Y, Zhang W, Niu J, Chen Y. Mechanism of photogenerated reactive oxygen species and correlation with the antibacterial properties of engineered metal-oxide nanoparticles. *ACS Nano*. 2012;6(6):5164–5173.
23. Jin SE, Ahn HS, Kim JH, et al. Boiling method-based zinc oxide nanorods for enhancement of adipose-derived stem cell proliferation. *Tissue Eng Part C Methods*. 2016;22(9):847–855.
24. Yu X, Marks TJ, Facchetti A. Metal oxides for optoelectronic applications. *Nat Mater*. 2016;15(4):383–396.
25. Arakha M, Saleem M, Mallick BC, Jha S. The effects of interfacial potential on antimicrobial propensity of ZnO nanoparticle. *Sci Rep*. 2015;5:9578.
26. Leung YH, Xu X, Ma AP, et al. Toxicity of ZnO and $TiO_2$ to Escherichia coli cells. *Sci Rep*. 2016;6:35243.
27. Hajipour MJ, Fromm KM, Ashkarran AA, et al. Antibacterial properties of nanoparticles. *Trends Biotechnol*. 2012;30(10):499–511.
28. Djurišić AB, Leung YH, Ng AM, Xu XY, Lee PK, Degger N, Wu RS. Toxicity of metal oxide nanoparticles: mechanisms, characterization, and avoiding experimental artefacts. *Small*. 2015;11(1):26–44.
29. Liu C, Zhang J, Peng L, et al. Hierarchical macro- and mesoporous assembly of metal oxide nanoparticles derived from metal-organic complex. *Microporous and Mesoporous Materials*. 2015;217:6–11.
30. Jana TK, Maji SK, Pal A, Maiti RP, Dolai TK, Chatterjee K. Photocatalytic and antibacterial activity of cadmium sulphide/zinc oxide nanocomposite with varied morphology. *J Colloid Interface Sci*. 2016;480:9–16.
31. Wattanawikkam C, Pecharapa W. Sonochemical synthesis, characterization, and photocatalytic activity of perovskite $ZnTiO_3$ nanopowders. *IEEE Trans Ultrason Ferroelectr Freq Control*. 2016;63(10):1663–1667.
32. Pei LZ, Yin WY, Wang JF, et al. Low temperature synthesis of magnesium oxide and spinel powders by a sol-gel process. *Materials Research*. 2010;13(3):339–343.
33. Yang C, Xiao F, Wang J, Su X. Synthesis and microwave modification of CuO nanoparticles: Crystallinity and morphological variations, catalysis, and gas sensing. *J Colloid Interface Sci*. 2014;435:34–42.
34. Gopinath V, Priyadarshini S, Al-Maleki AR, et al. In vitro toxicity, apoptosis and antimicrobial effects of phyto-mediated copper oxide nanoparticles. *RSC Adv*. 2016;6:110986.
35. Zhang H, Ji Z, Xia T, et al. Use of metal oxide nanoparticle band gap to develop a predictive paradigm for oxidative stress and acute pulmonary inflammation. *ACS Nano*. 2012;6(5):4349–4368.
36. Dhawan A, Sharma V. Toxicity assessment of nanomaterials: methods and challenges. *Anal Bioanal Chem*. 2010;398(2):589–605.
37. Sirelkhatim A, Mahmud S, Seeni A, et al. Review on zinc oxide nanoparticles: antibacterial activity and toxicity mechanism. *Nano Micro Lett*. 2015;7(3):219–242.
38. Kar S, Gajewicz A, Roy K, Leszczynski J, Puzyn T. Extrapolating between toxicity endpoints of metal oxide nanoparticles: Predicting toxicity to Escherichia coli and human keratinocyte cell line (HaCaT) with Nano-QTTR. *Ecotoxicol Environ Saf*. 2016;126:238–244.
39. McBriarty ME, von Rudorff GF, Stubbs JE, Eng PJ, Blumberger J, Rosso KM. Dynamic stabilization of metal oxide-water interfaces. *J Am Chem Soc*. 2017;139(7):2581–2584.
40. Mu R, Zhao Z, Dohnalek Z, Gong J. Structural motifs of water on metal oxide surfaces. *Chem Soc Rev*. 2017;46(7):1785–1806.
41. Ansari SA, Khan MM, Kalathil S, Nisar A, Lee J, Cho MH. Oxygen vacancy induced band gap narrowing of ZnO nanostructure by electrochemically active biofilm. *Nanoscale*. 2013;5(19):9238–9246.
42. Kalathil S, Khan MM, Ansari SA, Lee J, Cho MH. Band gap narrowing of titanium dioxide ($TiO_2$) nanocrystals by electrochemically active biofilm and their visible light activity. *Nanoscale*. 2013;5(14):6323–6326.
43. Akhil K, Jayakumar J, Gayathri G, Khan SS. Effect of various capping agents on photocatalytic, antibacterial and antibiofilm activities of ZnO nanoparticles. *J Photochem Photobiol B*. 2016;160:32–42.
44. Wang L, Hu C, Shao L. The antimicrobial activity of nanoparticles: present situation and prospects for the future. *Int J Nanomedicine*. 2017;12:1227–1249.
45. Reyes B, Gasmuri C, Estenoz L, Mora Y, ALvarez D, Beldarrain A. Strategies for the assessment of disinfection and cleaning on biopharmaceutical cleanroom. *Adv Biomed Eng Res*. 2014;2:18–27.
46. Hassana MS, Amna T, Yang OB, El-Newehy MH, Al-Deyab SS, Khil MS. Smart copper oxide nanocrystals: synthesis, characterization, electrochemical and potent antibacterial activity. *Colloids Surf B Biointerfaces*. 2012;97:201–206.